Vibrational Population Relaxation and Dephasing Dynamics of $Fe(CN)_6^{4-}$ in D_2O with Third-Order Nonlinear Infrared Spectroscopy

Kaoru Ohta,[†] Hiroaki Maekawa,[†] and Keisuke Tominaga*[,†,‡,§]

Graduate School of Science and Technology and Molecular Photoscience Research Center, Kobe University, Nada-ku, Kobe 657-8501, Japan, and CREST/JST

Received: October 5, 2003; In Final Form: December 15, 2003

Third-order nonlinear IR spectroscopy has been used to study the vibrational population relaxation and the vibrational dephasing dynamics of the CN stretching mode of $Fe(CN)_6^{4-}$ in D_2O. Transient-grating signals in the magic-angle condition show a biexponential decay upon the excitation of the T_{1u} mode of the CN stretching motion. A fast-decaying component (∼700 fs) of the transient-grating signal is attributed to the rapid equilibration between the T_{1u} mode and the Raman-active modes. The time scale of the slow-decaying component is around 23 ps, which corresponds to the vibrational population relaxation from the $v = 1$ state of the CN stretching mode. Anisotropy of the transient-grating signal decays with a time constant of 2.6 ps, which is due to the time evolution of the superposition states of the triply degenerate T_{1u} modes. Three-pulse photon-echo measurements showed that the correlation function of the frequency fluctuations decays biexponentially with time constants of 80 fs and 1.5 ps. The time scales of the decay of the correlation function are similar to those for SCN^- in D_2O even though the coupling strength of the solute−solvent interaction depends on the systems. On the basis of these results, we discuss the vibrational dynamics of the CN stretching mode of $Fe(CN)_6^{4-}$ in D_2O.

1. Introduction

In the condensed phase, the line width of the vibrational spectrum is broader than that in the gas phase. Vibrational line shapes contain information on the dynamical interaction with the environment.[1,2] Traditionally the mechanism of the broadening has been classified into two; a rapid modulation of the energy gap between the ground and excited states occurs by the interaction with the neighboring solvent molecules (homogeneous broadening). Furthermore, each solute molecule sometimes has different transition frequency due to the heterogeneity of the local structure of the solute−solvent configuration (inhomogeneous broadening). From the line shape analysis of the linear absorption spectrum, we could extract information on the broadening mechanism in principle.[3,4] However, it always has certain ambiguity in separating various contributions to the line shape. Vibrational photon-echo spectroscopy has been shown to be a powerful tool to eliminate static inhomogeneous broadening contributions from the line shape of the vibrational spectrum, particularly when there is clear distinction of the time scales between the fast- and slow-frequency modulations of the vibrational transition.[5] Fayer and co-workers used a two-pulse photon-echo method to study the vibrational dephasing in liquids, polymer, and proteins.[6−8] Combined with the results of the polarization sensitive pump−probe and transient-grating experiments, they separated the contribution of pure dephasing, population relaxation, and orientational relaxation from the line shape of the absorption spectrum.[6]

In room-temperature solution, the spectral diffusion process or solvation dynamics often occurs on multiple time scales and cannot be described by a single time constant.[9] Three-pulse photon-echo experiment is a useful technique to probe such a spectral diffusion process with multiple time scales.[9] This method has been used to determine the vibrational frequency correlation functions for small molecules in solutions and protein environments.[10−12] In the case of the vibrational transition, the time scale of the vibrational dephasing is sometimes similar to that of the vibrational population relaxation and/or the rotational relaxation. These processes take place on a picosecond time scale for small polyatomic molecules. In some cases, the dephasing process is dominated by the population relaxation. For example, a sub-picosecond decay in the vibrational population relaxation was observed for the C═O stretching mode of acetic acid dimer[13] and the antisymmetric stretching of the N═C═N bond.[14] On the basis of the stimulated photon-echo measurement, vibrational dephasing occurs on a similar time scale to the vibrational population relaxation. In this case, vibrational population relaxation plays an important role in the dephasing process. Therefore, it is important to obtain information on not only the vibrational frequency correlation function but also the vibrational population relaxation time and rotational relaxation time for characterizing the vibrational dynamics in the condensed phase. Pump−probe and/or transient-grating methods with the polarized lights provide information on the population dynamics such as the vibrational population relaxation time and orientational relaxation.

Recent experimental studies of the vibrational dynamics on small ions in water provide information on the mechanism of the vibrational dynamics,[10,15−18] which have stimulated theoretical studies. Hamm et al. used a three-pulse photon-echo method to determine the correlation function of the vibrational energy fluctuations for N_3^- in D_2O and found that the correlation function decays with time constants of 80 fs and 1.3 ps.[10] The slow-decaying component of the correlation function was

* Author to whom correspondence may be addressed. E-mail: tominaga@kobe-u.ac.jp. Phone: +81−78−803−5684. Fax +81−78−803−5684.
[†] Graduate School of Science and Technology, Kobe University.
[‡] Molecular Photoscience Research Center, Kobe University.
[§] CREST/JST.

10.1021/jp0369847 CCC: $27.50
Published on Web 02/03/2004

attributed to the dynamics of the hydrogen bonds.[19] The time scale of the fast-decaying component was pointed out to be similar to the inertial component of the solvation dynamics. We also performed three-pulse photon-echo measurements for the antisymmetric stretching of OCN^- and SCN^- in methanol.[20] The correlation function of the vibrational frequency fluctuation decays with a bimodal feature. The slower decay of the correlation function is around 4 ps, which is slower than that of N_3^- in D_2O. It was found that the amplitude of the coupling strength to the solvent for SCN^- is larger than that for OCN^- while the time scale of the frequency fluctuation is similar for the both cases.

In this paper, we have investigated the vibrational population relaxation and vibrational dephasing of the CN stretching mode for $Fe(CN)_6^{4-}$ in D_2O with third-order IR nonlinear spectroscopy. $Fe(CN)_6^{4-}$ belongs to the O_h point group, and the IR-active CN stretching modes are triply degenerate. A direction of the antisymmetric motion of the triply degenerate CN stretching mode (T_{1u} mode) is orthogonal to each other. The T_{1u} mode is an antisymmetric CN stretching motion of the opposite in-line CN pairs. Fayer and co-workers made comprehensive work on vibrational dynamics of the CO stretching mode of $W(CO)_6$ by third-order nonlinear-IR spectroscopy.[6,21,22] For such a system, it is important to understand not only the vibrational population relaxation from the T_{1u} mode to other intramolecular or intermolecular modes but also the time evolution of the population distribution process among the three states of the T_{1u} mode, which could affect the vibrational dephasing process. Furthermore, solute−solvent interactions for the T_{1u} mode lead to symmetry breaking of the triply degenerate mode, that might cause unique dephasing mechanism which does not exist for the nondegenerate system. We have performed transient-grating measurements to investigate the vibrational population relaxation. We have also measured the polarization dependence of the transient-grating signals to separate the depolarization dynamics from the population relaxation. Three-pulse photon-echo measurements are carried out to determine the correlation function of the vibrational frequency fluctuations. For comparison of the vibrational dephasing dynamics, we have also performed the three-pulse photon-echo measurements on the anti-symmetric stretching mode of SCN^- in D_2O.

2. Experimental Section

The apparatus for the three-pulse IR photon-echo measurement has been described previously.[20] Briefly, a tunable femtosecond IR pulse was generated by difference frequency mixing between the signal and idler of the optical parametric amplifier in a $AgGaS_2$ crystal. A mid-IR pulse has a 140−200-fs pulse width and a 120−130 cm^{-1} bandwidth with a repetition rate of 1 kHz.[23] The IR beam was split into three and was focused at the sample in a boxcar geometry. Two of them were delayed with the stepper motor translation stages. The photon-echo signal was detected with a liquid N_2 cooled InSb detector in the phase-matched direction $-\mathbf{k_1} + \mathbf{k_2} + \mathbf{k_3}$, where $\mathbf{k_1}$, $\mathbf{k_2}$, and $\mathbf{k_3}$ are the wavevectors of the first, second, and third pulses, respectively. The time sequence is defined as τ and T where τ is the time interval between the $\mathbf{k_1}$ and $\mathbf{k_2}$ beams while T is the time interval between the $\mathbf{k_2}$ and $\mathbf{k_3}$ beams for $\tau > 0$ or between $\mathbf{k_1}$ and $\mathbf{k_3}$ beams for $\tau < 0$. The polarization of the laser pulses was controlled with wire-grid polarizers. For the measurement of frequency-resolved photon-echo signals, the signals were dispersed in a monochromator and then detected with a liquid N_2 cooled InSb detector. The resolution of the monochromator is set to 3.5 cm^{-1}. The echo spectrum was measured by scanning the monochromator at particular delay times τ and T.

For measurements of the steady-state Raman spectrum, a 488-nm line from an Ar^+ ion laser was used for the excitation. The Raman scattering at 90° was collected and dispersed with a double monochromator. The Raman spectrum was detected with a CCD detector.

$K_4[Fe(CN)_6]\cdot 3H_2O$ and KSCN was purchased from WAKO Pure Chemical Industries, and D_2O was purchased from Aldrich. Both were used without further purification. The sample was 27 mM solution for $Fe(CN)_6^{4-}$ and 235 mM for SCN^- in a CaF_2 cell with an optical path length of 25 μm. All measurements were performed at ambient temperature (295 K).

3. Theoretical Background

IR photon-echo and transient-grating methods are time-domain nonlinear techniques based on the third-order nonlinearity of the optical polarization. A third-order nonlinear optical signal is expressed by integrating the polarization with respect to t which is given as follows

$$I(\tau,T) = \int_0^\infty |P(t,T,\tau)|^2 \, dt \tag{1}$$

where P is the third-order nonlinear polarization. Third-order polarization is expressed by the convolution of the response function, $R(t_1,t_2,t_3)$, with the electric fields of the laser pulses[24]

$$P^{(3)}_i(t,T,\tau) = \int_0^\infty dt_3 \int_0^\infty dt_2 \int_0^\infty dt_1 R_{ijkl}(t_1,t_2,t_3) E_{3j}(t-t_3) \times E_{2k}(t+T-t_3-t_2) E_{1l}(t+T+\tau-t_3-t_2-t_1) \tag{2}$$

Here i, j, k, and l are the laboratory frame orientational indices. In the analysis, the states of the triply degenerate T_{1u} modes are regarded as one state, which assumes the fluctuations of the three states are the same and coherence between two states among the three is neglected. However, in a real situation, an anisotropic interaction between the solute and the solvent leads to the symmetry breaking of the degeneracy of the T_{1u} mode as described in the section 5.2. The effect of the coherence between the two different modes is not negligible in the total nonlinear response in the case the intermode coupling is large enough. An example is the coupling between two strongly coupled CO stretching modes for $Rh(CO)_2(C_5H_7O_2)$.[25−27] In this system, the intermode coupling is so strong that the energy splitting of the symmetric and asymmetric stretching modes is larger than the line width of the absorption spectrum and two peaks of the symmetric and asymmetric stretching modes are clearly separated. In our system, the amount of the energy splitting due to this anisotropic interaction is much smaller than the line width of the absorption spectrum of the T_{1u} mode. Therefore the line width of the absorption spectrum is mainly determined by dynamic fluctuation of the solvent environment. Furthermore, as shown in the later section, the time evolution of the superposition of the three states is considered to take place with a time constant of 2.6 ps based on the anisotropy decay. This rate is not so fast compared to decay of the photon-echo signals. These facts suggest that the anharmonic coupling among the triply degenerate T_1 modes, which may be due to anisotropic coupling between the solute and solvent, may be small. Consequently, we adopt a model for the analysis based on a single vibrational oscillator coupled with the bath and phenomenological description of the anisotropy decay of the nonlinear signals. However, full theoretical treatment based on the three weakly coupled T_{1u} modes is necessary to interpret the experimental data, which will be addressed in a future study.

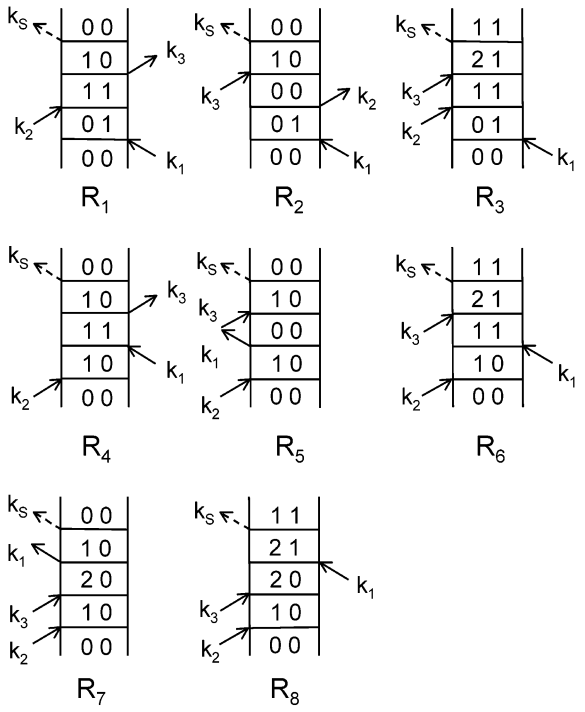

Figure 1. Double-side Feynman diagrams that contribute to the photon-echo signals.

In this model, we assume that the orientational motion is not coupled to the vibrational dynamics. This means that the response function can be described by the product of an isotropic vibrational response function and an orientational response function as follows[28]

$$R_{ijkl}(t_3,t_2,t_1) = Y_{ijkl}(t_3,t_2,t_1)\mathrm{G}(t_3,t_2,t_1) \tag{3}$$

where $Y_{ijkl}(t_3,t_2,t_1)$ is the orientational contribution to the response function and $G(t_3,t_2,t_1)$ is the isotropic part of the vibrational response function. The orientational response function depends on the polarization of the input electric fields. Assuming that the molecule is regarded as a spherical rotor, the orientational contribution of the polarization with the parallel and perpendicular polarizations is given by, respectively[28]

$$Y_{ZZZZ}(t_3,t_2,t_1) = \frac{1}{9}\exp(-2Dt_3)\left[1+\frac{4}{5}\exp(-6Dt_2)\right]\exp(-2Dt_1) \tag{4}$$

$$Y_{YYZZ}(t_3,t_2,t_1) = \frac{1}{9}\exp(-2Dt_3)\left[1-\frac{2}{5}\exp(-6Dt_2)\right]\exp(-2Dt_1) \tag{5}$$

where D is the diffusion constant of the orientational motion and the reorientational time is defined as

$$\tau_r = \frac{1}{6D} \tag{6}$$

A detailed description of the isotropic part of the response functions has been given in other papers.[10,24,29] Briefly, interaction of the system with the electric fields is expressed by Feynman diagrams. The response function is a sum of contributions from each of Feynman paths as shown in Figure 1. The first three diagrams contribute to the photon-echo signal when the delay time τ is positive. These are so-called rephasing diagrams which give photon-echo signals. The rest of the diagrams contribute to the signal when the delay time τ is negative. These are so-called nonrephasing diagrams which give free induction decays. The response functions, R_1, R_2, R_4, and R_5, involve only the coherence of the $v = 0-1$ transition propagating during the delay times τ and t. The response functions, R_3 and R_6, involve the coherence of the $v = 0-1$ transition propagating during τ and the coherence of the $v = 1-2$ transition propagating during t. R_7 and R_8 contribute to the signal only when T is close to zero.

For the transient-grating measurements, we set τ to zero. The time dependence of the transient-grating signals at the parallel and perpendicular polarizations of the pump and probe pulses in the impulsive limit is given by, respectively

$$I^{\parallel}_{\mathrm{TG}}(T) = I_0[N(T)]^2\left[1+\frac{4}{5}\exp(-6DT)\right]^2 \tag{7}$$

$$I^{\perp}_{\mathrm{TG}}(T) = I_0[N(T)]^2\left[1-\frac{2}{5}\exp(-6DT)\right]^2 \tag{8}$$

where $N(T)$ is the population of the $v = 1$ state at time T. As is well known, the transient-grating signals at the magic-angle condition contain only population dynamics, eliminating the orientational contribution to the signal. The anisotropy of the transient-grating signals can be calculated from the following equation

$$r(T) = \frac{(I^{\parallel}_{\mathrm{TG}}(T))^{1/2} - (I^{\perp}_{\mathrm{TG}}(T))^{1/2}}{(I^{\parallel}_{\mathrm{TG}}(T))^{1/2} + 2(I^{\perp}_{\mathrm{TG}}(T))^{1/2}} \tag{9}$$

For the photon-echo measurements, we measure the nonlinear optical signals by scanning the delay time τ at a certain T.[10,29] As shown in the previous studies, the three-pulse photon-echo signals provide information on the temporal evolution of the inhomogeneous distribution of the vibrational transition frequency. In the presence of the inhomogeneity, the integrated intensity becomes larger for $\tau > 0$ than that for $\tau < 0$.[9] As delay time T increases, spectral diffusion destroys the static inhomogeneity in the distribution of the vibrational frequencies. When there is no inhomogeneity in the system or the inhomogeneity is washed out completely due to the spectral diffusion, rephasing and nonrephasing diagrams contribute equally to the signals, and the photon-echo signal becomes symmetric with respect to $\tau = 0$ fs. Therefore, the asymmetry of the photon-echo signals is a sensitive probe of the degree of the inhomogeneity in the distribution of the vibrational frequencies.[10,29]

The distribution of the vibrational frequency fluctuations is characterized by the correlation function of the vibrational frequency fluctuations

$$M(t) = \langle \delta\omega_{01}(t)\delta\omega_{01}(0)\rangle \tag{10}$$

where $\delta\omega_{01}(t)$ is the shift of the vibrational frequency at time t from the average value. We calculate third-order nonlinear response functions from the line-broadening function, $g(t)$

$$g(t) = \int_0^t \mathrm{d}t_1 \int_0^{t_1} dt_2 \langle \delta\omega_{01}(t_2)\delta\omega_{01}(0)\rangle \tag{11}$$

Here we assume that the anharmonicity fluctuation is small so that $\delta\omega_{12}(t)$ is equal to $\delta\omega_{01}(t)$. In the following simulation, we take into account an effect of the finite pulse width, the population relaxation, and rotational relaxation. Contribution of each diagram R_1-R_8 depends on the time ordering of the three pulses and all of the diagrams are included in the calculation.

As shown later, the population relaxation occurs in a nonexponential fashion. We have to incorporate the nonexponential population kinetics in the response function. According to Lim and Hochstrasser,[13] we use the following term in the population decay from the $v = 1$ state in place of a single-exponential decay function

$$P_{11}(t) = \exp[-\int_0^t k_1(t')\,dt'] \tag{12}$$

where $k_1(t)$ is the time-dependent population decay rate from the $v = 1$ state. The population decay factors of the 0−1 coherence and 1−2 coherence during the time τ and t are given by

$$P_{01}(t) = \exp\left[-\frac{1}{2}\int_0^t k_1(t')\,dt'\right] \tag{13}$$

$$P_{12}(t) = \exp\left[-\frac{1}{2}\int_0^t \{k_1(t') + k_2(t')\}\,dt'\right] \tag{14}$$

where $k_2(t)$ is the time-dependent population decay rate from the $v = 2$ state. We assume that the population relaxation time from the $v = 2$ state is a half of that from the $v = 1$ state. This assumption is based on the harmonic approximation for the transition dipole moment, i.e., $2\mu_{10}^2 = \mu_{21}^2$. Transition rate is given by the Fermi's golden rule and is linear in the vibrational quantum number for the harmonic oscillator.[30]

4. Results

4.1. Linear IR and Raman Spectra. Figure 2 shows the linear IR absorption and Raman spectra of $Fe(CN)_6^{4-}$ in D_2O. For the IR spectrum, a single band with a peak at 2036 cm^{-1} was observed. Full width at half maximum of the absorption spectrum is around 16 cm^{-1}. The shape of the absorption spectrum is slightly asymmetric with a tail at high-frequency side. For the Raman spectrum, two bands appear at the parallel polarization. The peaks of the two bands are located at 2057 and 2094 cm^{-1}, respectively. For the perpendicular polarization, only one mode was observed at 2057 cm^{-1}. It is known that there are three different transitions near the 2000-cm^{-1} region for $Fe(CN)_6$.[4−31,32] $Fe(CN)_6^{4-}$ is considered to belong to the O_h point group. An IR-active mode is the T_{1u} mode, which is triply degenerate, while Raman-active modes are the E_g and A_{1g} modes, which are doubly degenerate and nondegenerate, respectively.[31,32] On the basis of the results of the Raman spectrum with different polarization conditions, a band at 2057 cm^{-1} is assigned to the E_g mode and a band at 2094 cm^{-1} to the A_{1g} mode.

4.2. Transient-Grating and Three-Pulse Photon-Echo Signals of $Fe(CN)_6^{4-}$. Figure 3 shows the transient-grating signals of $Fe(CN)_6^{4-}$ in D_2O at the parallel, perpendicular, and magic-angle polarization conditions of the pump and probe pulses. It should be noted that the amplitude of the transient-grating signal is proportional to a square of the excited-state population and ground-state hole. Therefore, single-exponential dynamics appears as a single-exponential decay with a time constant half of the lifetime, while biexponential dynamics appears as a square of biexponential exponential function for the population dynamics. For fitting of the transient-grating signal, we calculated a square root of the transient-grating signal first and then fitted it with a sum of the exponentials.[21]

For the parallel polarization, the transient-grating signal decays in a bimodal fashion. On the other hand, for the perpendicular condition, a fast rising component was observed on a picosecond time scale. After 10 ps, the transient-grating signals at the parallel and perpendicular polarizations closely overlap to each other, which decays on a 20-ps time scale. In the magic-angle condition, the slow-decaying component is dominant in the signal. We fitted the signal at the magic-angle

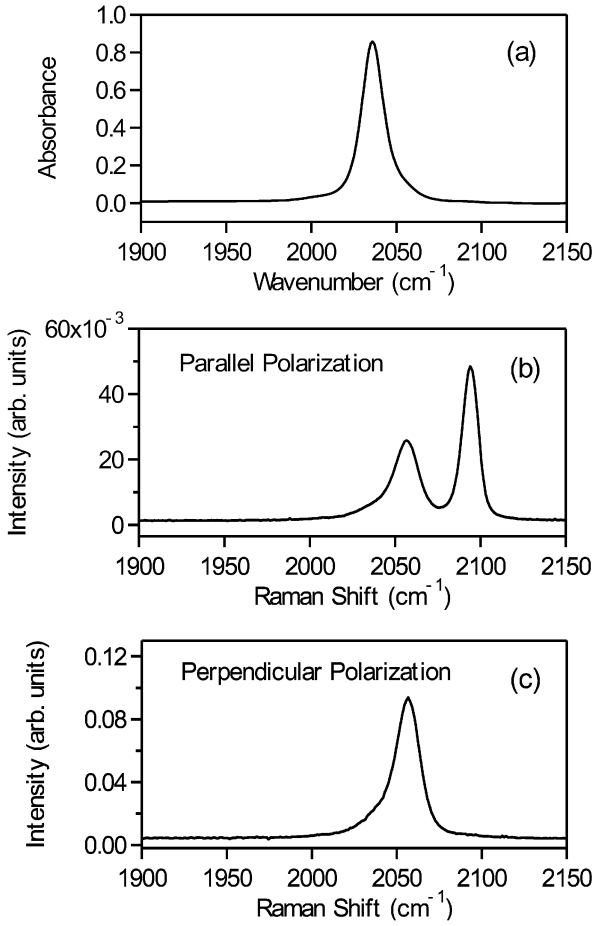

Figure 2. (a) Linear IR absorption spectrum of the CN stretching mode of $Fe(CN)_6^{4-}$ in D_2O. (b) Raman spectrum of the CN stretching mode of $Fe(CN)_6^{4-}$ in D_2O at the parallel polarization condition. (c) Raman spectrum of the CN stretching mode of $Fe(CN)_6^{4-}$ in D_2O at the perpendicular polarization condition.

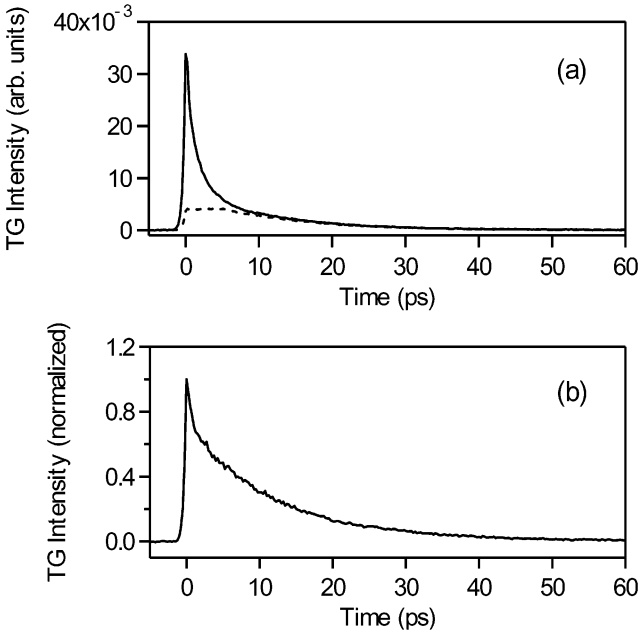

Figure 3. (a) Transient-grating signals of $Fe(CN)_6^{4-}$ in D_2O at the parallel (solid line) and perpendicular (dashed line) polarization. (b) Transient-grating signal of $Fe(CN)_6^{4-}$ in D_2O at the magic-angle condition.

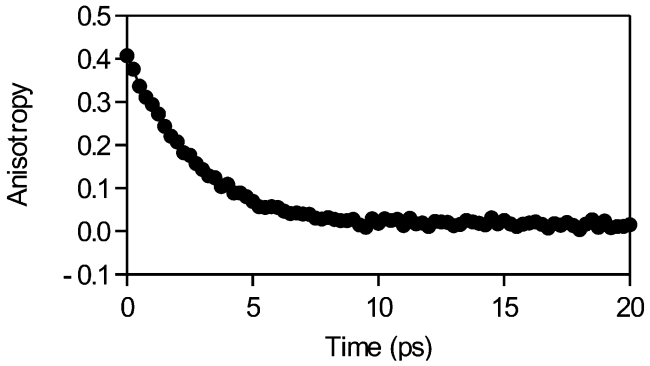

Figure 4. Anisotropy decay calculated from the experimental data of the transient-grating signals at the parallel and perpendicular polarization conditions.

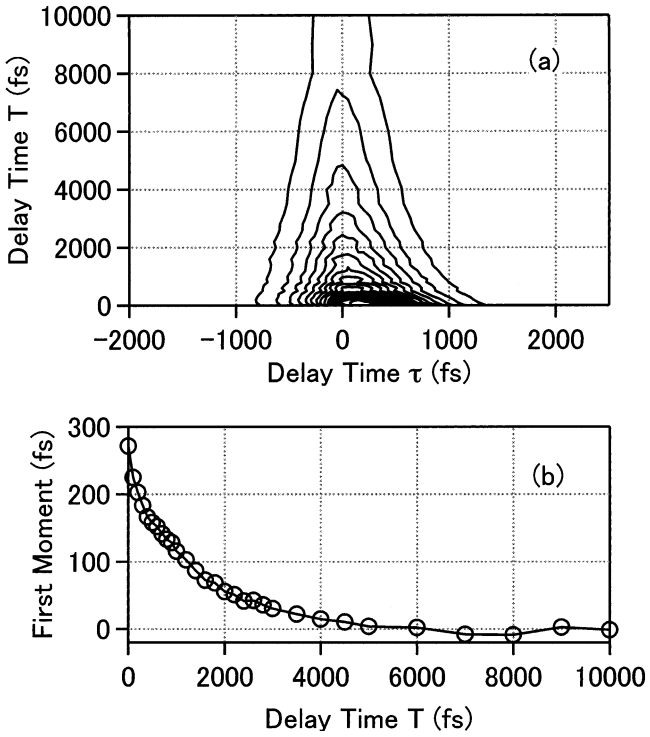

Figure 5. (a) Three-pulse photon-echo signals plotted against the delay times τ and T for $Fe(CN)_6^{4-}$ in D_2O. (b) The first moment of the photon-echo signals from the experimental data (solid line with open circles).

condition with a square of a double exponential. The decay time constants of the fast and the slow components are 0.7 and 23.0 ps, respectively. The anisotropy of the transient-grating signal is shown in Figure 3. The initial anisotropy starts at near 0.4 and decays with a time constant of 2.6 ps.

Figure 5a displays the three-pulse photon-echo signals of $Fe(CN)_6^{4-}$ in D_2O at the parallel polarization condition. At $T = 0$ fs, the peak of the photon-echo signal is located at around 150−200 fs. The temporal profile of the photon-echo signal is highly asymmetric with respect to τ. This is due to the presence of the inhomogeneous distribution of the vibrational frequency. The peak of the signal shifts toward zero as T increases. To characterize the degree of asymmetry of the photon-echo signals, the first moments of the echo signals are calculated against the delay time T as shown in Figure 5b. The first moment is defined as follows[10,29]

$$FM(T) = \frac{\int_{-\infty}^{\infty} \tau I(\tau,T)\, d\tau}{\int_{-\infty}^{\infty} I(\tau,T)\, d\tau} \qquad (15)$$

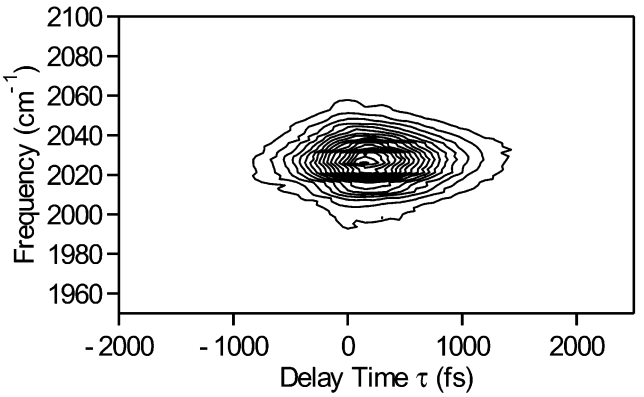

Figure 6. Frequency-resolved photon-echo signals plotted against the delay time τ and the frequency for $Fe(CN)_6^{4-}$ in D_2O measured at $T = 0$ fs.

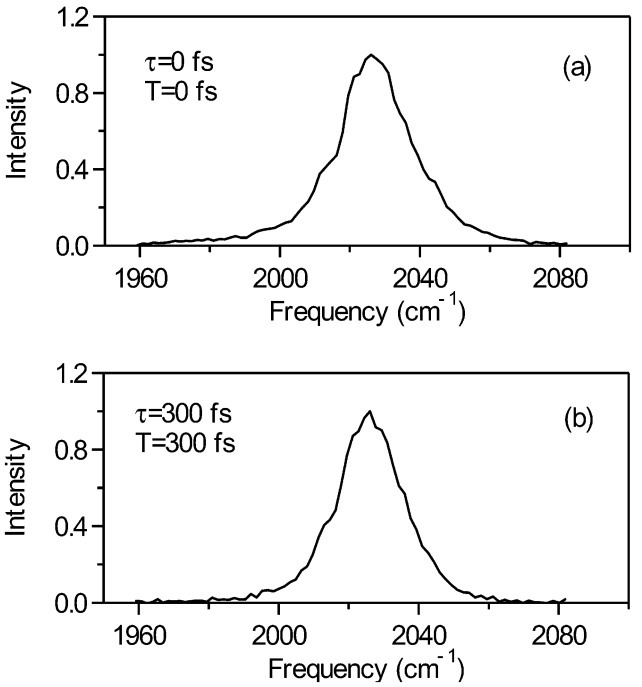

Figure 7. Frequency-resolved photon-echo spectra of $Fe(CN)_6^{4-}$ in D_2O (a) at $\tau = 0$ fs, $T = 0$ fs and (b) at $\tau = 300$ fs, $T = 300$ fs.

where $I(\tau,T)$ is the experimental photon-echo signal at the delay times τ and T. The first moment decays on a 1.5-ps time scale and is close to zero at $T = 10$ ps.

4.3. Frequency-Resolved Photon-Echo Signals of $Fe(CN)_6^{4-}$. Figure 6 shows the result of the frequency-resolved three-pulse photon-echo signals of $Fe(CN)_6^{4-}$ in D_2O at $T = 0$ fs. The peak of the signals is located at around 150 fs and 2025−2030 cm^{-1}. As shown in the previous studies, the frequency-resolved measurements allow the separation of contributions from different Feynman pathways to the echo signals such as the contributions from the 0−1 and 1−2 coherence terms.[33,34] Separation of the two peaks originating from the 0−1 and 1−2 coherence terms is given by the anharmonicity. In our case, two peaks are not clearly resolved because the magnitude of anharmonicity is comparable with the line width of the absorption spectrum. Figure 7 shows the one-dimensional slice of the photon-echo spectra at $\tau = 0$ fs and $T = 0$ fs, and $\tau = 300$ fs and $T = 300$ fs. Spectral feature of the echo signals at different delay times τ and T is similar to each other.

4.4. Three-Pulse Photon-Echo Signals of SCN^- in D_2O. For comparison, we also measured the three-pulse photon-echo

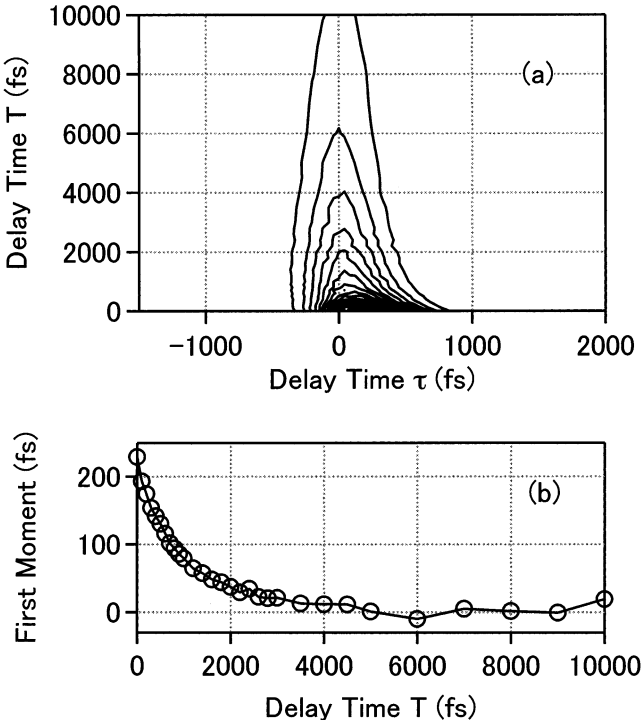

Figure 8. (a) Three-pulse photon-echo signals plotted against the delay times τ and T for SCN^- in D_2O. (b) First moment of the photon-echo signals from the experimental data (solid line with open circles).

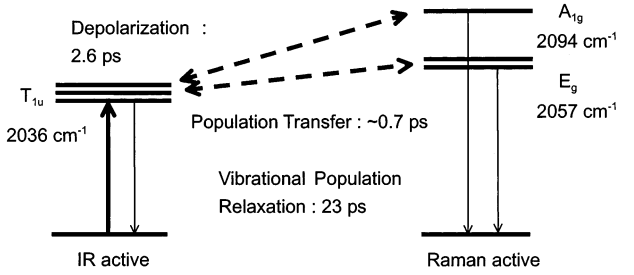

Figure 9. Summary of the vibration population relaxation process of $Fe(CN)_6^{4-}$ in D_2O.

signals for the antisymmetric stretching mode of SCN^- in D_2O. On the basis of the normal-mode analysis of the ab initio calculation, it is shown that a vibration of the antisymmetric stretching is localized on the CN stretching mode in SCN^-.[17,20] Figure 8a shows the three-pulse photon-echo signals of SCN^- in D_2O as a function of delay times τ and T. At $T = 0$ fs, the peak of the photon-echo signal is located at around 150−200 fs. The peak of the signals shifts toward zero as T increases. Figure 8b displays the first moment of the photon-echo signals plotted against the delay time T. As similar to $Fe(CN)_6^{4-}$ in D_2O, the first moment for SCN^- decays on a 1.5-ps time scale and is close to zero at $T = 10$ ps. Temporal width of the photon-echo signal for SCN^- with respect to the delay time T is narrower than that for $Fe(CN)_6^{4-}$ This is due to a stronger system-bath interaction for SCN^- compared to $Fe(CN)_6^{4-}$ as we will discuss in the next section.

5. Discussion

5.1. Population Dynamics. A summary of the vibrational population dynamics based on the transient-grating measurements is shown in Figure 9. A decaying component of the transient-grating signal on a few picosecond time scale is sensitive to the polarization of the pump and probe pulses. The anisotropy decay is often due to the physical rotation of the molecule itself. The reorientational times of small ions such as CN^-, N_3^-, and SCN^- in water were determined by the anisotropy measurements of IR pump−probe experiments.[15,17] A time constant of the anisotropy decay is around 1 ps for CN^- in water, while it is 7.1 and 4.7 ps for N_3^- and SCN^- in D_2O, respectively.[15,17] Though details of the reorientational dynamics of $Fe(CN)_6^{4-}$ in D_2O are not known, the time scale of 2.6 ps is too short for the reorientational dynamics of this system.

Another possibility for the anisotropy decay is due to symmetry breaking of the complex. $Fe(CN)_6^{4-}$ has an O_h symmetry, and the T_{1u} mode of the CN stretching is triply degenerate. However, coupling with other intramolecular modes and/or fluctuations of the surrounding solvents will break the triple degeneracy, yielding three modes with small energy splitting. The symmetry breaking causes the anisotropy decay of the T_{1u} mode through two different mechanisms. One mechanism is population transfer and/or dephasing among the three states of the T_{1u} mode.[21,35] The asymmetric stretching modes of the three pairs of cyanide ligands are directed along the three axes of the orthogonal coordinate system, *x*, *y*, and *z*. Excitation with the polarized light creates a certain superposition state among the three different states. Fluctuations of the solvent environment and other intramolecular modes with a certain symmetry cause changes of both energy separation and anharmonic coupling interactions among the three levels.[35] Such interactions with the T_{1u} modes induce the transition from one state of the T_{1u} modes to the others or pure dephasing. Thus the direction of the transition dipole changes as a function of time because the composition of the population distribution along the three different axes changes, causing the depolarization of the transient-grating signals. Therefore, the time evolution of the superposition states of the triply degenerate T_{1u} mode is regarded as the reorientational relaxation of the initial excited dipoles. Depolarization dynamics was observed in the vibrational transition of the T_{1u} mode of the asymmetric CO stretching mode of $W(CO)_6$ in several liquids.[21] They found that the temperature dependence on the orientational relaxation times is small even though the viscosity changes orders of magnitude in the range of the temperature they investigated.

The other mechanism is inhomogeneous energy splitting effects on the anisotropy decay.[36,37] Because of the weak distortion from the symmetry, energy separation between the three different levels is distributed within a certain range. Destructive interference of the coherent oscillations with different frequencies among the three levels leads to the rapid decay of the anisotropy. In this case, no population transfer or pure dephasing is included in the anisotropy decay. The fact that the anisotropy decay can be fitted with a single exponential indicates that the either mechanism is dominant or both the mechanisms occur on similar time scales. However, we cannot assign which mechanism is dominant for the present case.

Even in the magic-angle condition, we observed the fast-decaying component (∼0.70 ps) in the transient-grating signals. For $W(CO)_6$ in CCl_4, Tokmakoff et al. observed a fast phonon-induced scattering (∼1 ps) from the IR-active T_{1u} mode at 1980 cm^{-1} to the Raman-active E_g mode at 2012 cm^{-1} but not to the A_{1g} mode at 2116 cm^{-1} using picosecond IR pump/anti-Stokes Raman probe experiments.[38] In our case, the fast-decaying component can be attributed to the population equilibration between the T_{1u} mode and the Raman-active E_g and A_{1g} modes since the energy difference between IR-active mode and Raman-active mode is small. Frequency differences between the T_{1u} and E_g modes, and between the T_{1u} and A_{1g} modes for $Fe(CN)_6^{4-}$ in D_2O, are 21 and 58 cm^{-1}, respectively. Therefore

we can consider that the population transfer to a higher energy level is feasible, which is assisted by the low-frequency motions of the solvent. By use of a femtosecond IR pulse, we could obtain a time constant of this energy transfer to be 0.70 ps. A faster population transfer to the upper states for $Fe(CN)_6^{4-}$ in D_2O than for $W(CO)_6$ in CCl_4 may result from a couple of reasons. The first one is that the energy difference between the IR- and Raman-active modes for $Fe(CN)_6^{4-}$ is smaller than that for $W(CO)_6$. It may be also due to the different strengths of the anharmonic coupling between the IR- and Raman-active modes and/or the different densities of states for the low-frequency solvent modes.

From the decay of the transient-grating signal at the magic-angle condition, the vibrational relaxation of the $v = 1$ state from the T_{1u} mode occurs on 23.0 ps. The population of the initial excited vibrational mode will be equilibrated with the other CN stretching modes of different symmetries as pointed out in the previous section. It can also relax by transferring energy to a combination of the lower-frequency internal vibrations of the solute molecules and solvent phonon vibrational modes. Given the vibrational frequency of the solute and solvents, at least two other vibrations and a phonon of the solvent have to be excited in the course of the vibrational relaxation of the T_{1u} mode. According to the results of the ab initio calculation of $Fe(CN)_6^{4-}$, we can classify the three types of the lower-frequency modes of $Fe(CN)_6$.[4-39] There are six Fe−C stretching modes, nine angle-deformation modes for angled C−Fe−C bending, and twelve linear-angle-deformation modes for the linear Fe−CN bending. The frequencies of these modes are below ~600 cm^{-1} based on the results of the ab initio calculation. The frequency of the bending mode of D_2O is around 1210 cm^{-1}. Therefore the initial excitation of the T_{1u} mode may transfer the energy to the stretching and bending motion of $Fe(CN)_6^{4-}$, the bending motion of D_2O, and a solvent phonon that makes up for the energy mismatch. It should be noted that the population relaxation of the Raman-active modes also affects the vibrational relaxation of the T_{1u} mode in an indirect way, since the Raman-active CN stretching modes are in equilibrium with the T_{1u} mode. We are currently investigating isotope effect of solvents on the vibrational population relaxation to study the role of the solvent modes in the vibrational dynamics.[40]

5.2. Spectral Diffusion Process. From the measurements of the three-pulse photon-echo signals as a function of delay times τ and T, we can obtain information on the correlation function of the vibrational frequency fluctuation. To determine the magnitudes and time scales of the fluctuations, we simulated the photon-echo signals. The correlation function of the vibrational frequency fluctuation is assumed to be a sum of exponentials plus a constant

$$M(t) = \sum_{i=1}^{2} \Delta_i^2 \exp(-t/\tau_i) + \Delta_0^2 \qquad (16)$$

We assume that the depolarization dynamics with a 2.6-ps time constant is regarded as orientational relaxation of a spherical rotor. We calculated the temporal profile of the photon-echo signal at each delay time T according to eq 1, taking into account the pulse width and the time ordering of the laser pulses, and then the first moment of the photon-echo signal was calculated based on eq 15. The pulse shape was assumed to be a Gaussian function, which was incorporated in the calculation of the integral of eq 2. The population decay from the $v = 1$ state and the population decay factors of the 0−1 coherence and 1−2 coherence were obtained from the double exponential decay of the population dynamics at the magic-angle condition whose parameters are given in Table 1. Comparison of calculated signals with the experimental results for $Fe(CN)_6^{4-}$ in D_2O is displayed in Figure 10. The parameters used in the simulation are shown in Table 1. *M(T)* decays with time constants of 80 fs and 1.5 ps. We also calculated a linear absorption spectrum along with the experimental absorption spectrum (Figure 10d). The absorption spectrum is calculated from the following equation[10,29]

$$I(\omega) = 2\,\mathrm{Re}\int_0^\infty \exp[-i(\omega - \omega_{01})t]\exp[-g(t) - 2Dt] \times P_{01}(t)dt \qquad (17)$$

where $P_{01}(t)$ is the population relaxation factor in the 0−1 coherence. $P_{01}(t)$ was calculated from eq 13.

Good agreement between the experimental results and the simulation is obtained, however, we have a certain difference between the experimental and simulated results. The calculated absorption spectrum slightly overestimates the width of the experimental absorption spectrum. There are a couple of sources which give rise to the disagreement between the experiments and simulation. One of the reasons is that a small fifth-order polarization contributes to the photon-echo signals.[41] This is evident from the small shoulder near the 2000-cm^{-1} region as shown in Figure 6. The fifth-order contribution gives a shoulder in the spectrum at the lower-frequency side, which is due to the $v = 2-3$ coherence, and gives a small oscillatory feature due to the interference between the third-order and fifth-order optical polarization.[33] Small deviation of the calculated photon-echo signals from the experimental results may be due to the fifth-order contribution. For the fast-decaying components in $M(T)$, a product of $\Delta_1\tau_1$ is ~0.22 ≪ 1. This indicates that the fast process is close to the motional narrowing limit that would be described by a pure dephasing time, $(\Delta_1^2\tau_1)^{-1} = 1.6$ ps.

We also simulated the results of the three-pulse photon-echo signals for SCN^- in D_2O along with the linear absorption spectrum. Comparison of calculated signals with the experimental results for SCN^- in D_2O is displayed in Figure 11. $M(T)$

TABLE 1: Parameters of the Correlation Function of the Vibrational Frequencies, Vibrational Population Relaxation Times, Rotational Diffusion Constants, and Anharmonicities for $Fe(CN)_6^{4-}$, SCN^-, and N_3^- in D_2O as Well as OCN^- and SCN^- in Methanol

solutes	Δ_1 (ps^{-1})	τ_1 (ps)	Δ_2 (ps^{-1})	τ_2 (ps)	Δ_0 (ps^{-1})
$Fe(CN)_6^{4-}$[a]	2.8	0.08	1.15	1.5	0.0
SCN^-[a]	4.3	0.08	2.7	1.3	0.0
N_3^-[b]	2.6	0.08	1.4	1.3	0.3
OCN^-/methanol[c]	1.3	0.12	1.6	4.5	0.55
SCN^-/methanol[c]	2.6	0.09	3.6	4.1	0.1

solutes	T_1 (ps)	rotational diffusion constant (ps^{-1})	anharmonicity (cm^{-1})[f]
$Fe(CN)_6^{4-}$[a]	0.70 (17%) 23.0 (83%)	0.064[e]	15
SCN^-[d]	18.3	0.035	23

[a] This study. [b] Taken from ref 10. [c] Taken from ref 20. [d] Taken from ref 17. [e] Rotational diffusion constant for $Fe(CN)_6^{4-}$ is calculated from $D = 1/6\tau_{aniso}$ where τ_{aniso} is the time constant of the anisotropy decay of the transient-grating signals. [f] Value of the anharmonicity is estimated from the simulation of the frequency-resolved photon-echo signals. Because of the reabsorption of the echo signals by the sample itself, anharmonicity has a relatively large error compared to the other parameters. However, the result of the simulation is not so sensitive to the value of the anharmonicity. For SCN^-, the value of the anharmonicity is taken from the ref 17.

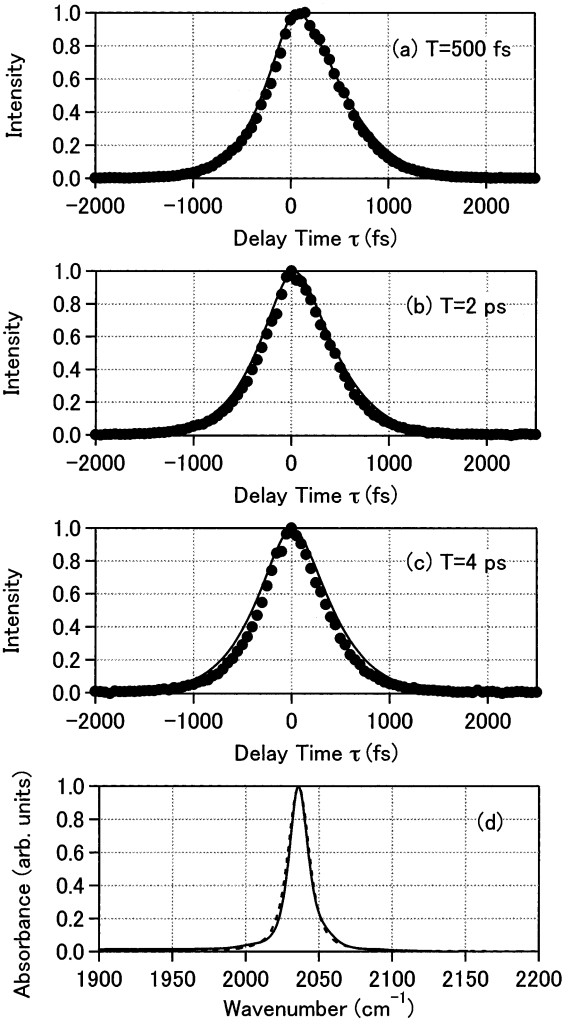

Figure 10. Three-pulse photon-echo signals of $Fe(CN)_6^{4-}$ in D_2O at three different delay times *T*: (a) 500 fs; (b) 2 ps; and (c) 4 ps. The filled circles represent the experimental data and the solid one represents the simulated data. (d) Experimental linear absorption spectrum of $Fe(CN)_6^{4-}$ in D_2O. The dashed line is calculated from the simulation using the parameters shown in Table 1.

decays with time constants of 80 fs and 1.3 ps, which is similar to that for $Fe(CN)_6^{4-}$ in D_2O, even though the amplitudes of the correlation function are different.

Table 1 summarizes one of the major conclusions of this work. The table also includes results on the triatomic ions in methanol. It can be seen that the time scales of the correlation function do not depend on the solute and are determined by the solvent, while the amplitudes of the components depend on the solute and solvent. In our previous work, we concluded that the time scale of the spectral diffusion of the triatomic ions in methanol is controlled by making and breaking of the hydrogen bond between the ion and solvent. Results of molecular dynamics simulations on CN^- and N_3^- in water and methanol indicated that the time scale of the hydrogen-bond dynamics in methanol is about three times longer than that in water. This was consistent with our experimental observations.[19,42] However, the molecular dynamics simulation also showed that the hydrogen-bonding dynamics is very sensitive to the charge distribution of the ion. Since the hydrogen-bond dynamics is short-range electrostatic interaction between the ion and solvent, it is readily understandable that a small change in the charge of the solute affects the time scale of making and breaking of the hydrogen bond. Although we do not have information on the charge distributions of the ions and an effect of their differences

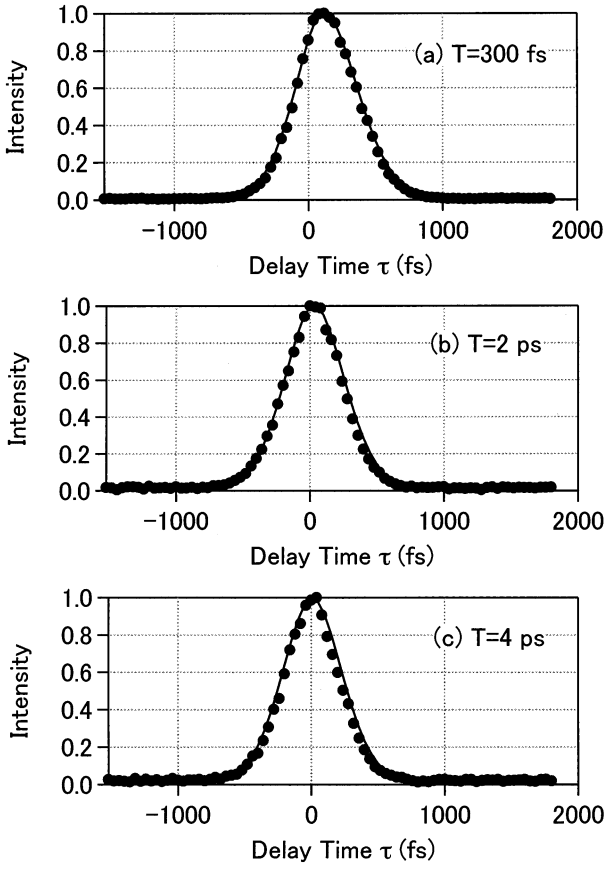

Figure 11. Three-pulse photon-echo signals of SCN^- in D_2O at three different delay times *T*: (a) 300 fs; (b) 2 ps; and (c) 4ps. The filled circles represent the experimental data and the solid one represents the simulated data.

on the hydrogen bond dynamics in a quantitative level, the experimental results show that the dynamics of the correlation function are mostly affected by the solvent nature. A longer-range interaction such as the electrostatic interaction between solute and solvent may be important for the vibrational frequency fluctuation in the present case.

So far, it has been argued whether the electrostatic interaction between the solute and solvent plays an important role in the vibrational dynamics in polar liquids such as vibrational population relaxation and frequency fluctuations by molecular dynamics simulations.[43,44] Especially, Morita and Kato emphasized importance of charge fluctuation induced by fluctuation of the external potential by the solvent in the vibrational relaxation of N_3^- in water.[45] Such a Coulombic force has a nature of long range, and the similar electrostatic interaction may play a role in the vibrational frequency fluctuation for the present case. Furthermore, a fast-decaying component of the correlation function has a similar time scale to that observed for the electronic transitions due to inertial motion of the solvent molecules. Our results suggested that the polarization fluctuations play an important role in the fast-decaying component of the correlation function of the vibrational frequency fluctuation similarly to the polar solvation dynamics studied in the electronic transition. It will be interesting to study how the solvation dynamics is correlated between the electronic transition and the vibrational transition.

The time scale of the correlation function for the vibrational frequency fluctuation for $Fe(CN)_6^{4-}$ in D_2O is similar to that for N_3^- and SCN^- in D_2O. This corresponds to similar time scales of the decaying components in *M(T)* for degenerate and nondegenerate systems. Fayer and co-workers showed that the

temperature dependence on the pure dephasing of $Rh(CO)_2(C_5H_7O_2)$ is different from that of $W(CO)_6$ in a same solvent.[35] They proposed that this difference results from the difference in mode degeneracy. For $W(CO)_6$, local fluctuations in solvent give rise to the energy separation among the triply degenerate modes, causing the dephasing mechanism that is not seen to $Rh(CO)_2(C_5H_7O_2)$. Even though the vibrational dephasing could be caused by both the energy gap fluctuation between the $v = 0$ and $v = 1$ states for the T_{1u} mode and the fluctuation of the energy splitting among the triply degenerate T_{1u} modes, our result suggested that the time scale of the spectral diffusion process for $Fe(CN)_6^{4-}$ is controlled by the same mechanism as that for SCN^-, not by the time-dependent anisotropic solute−solvent interaction. Further studies of the effects of the anisotropic fluctuations on the depolarization dynamics are necessary to understand the vibrational dynamics of the degenerate system in solution.

6. Concluding Remarks

In this paper, we have studied the vibrational population relaxation and the vibrational dephasing dynamics of the CN stretching mode for $Fe(CN)_6^{4-}$ in D_2O with third-order IR nonlinear spectroscopy. Upon the excitation of the triply degenerate T_{1u} mode of the CN stretching mode, the time evolution of the population distribution of the three orthogonal T_{1u} modes occurs on a 2.6-ps time scale, revealed by the polarization dependence of the transient-grating measurements. The vibrational population relaxation from the $v = 1$ state of the CN stretching mode occurs on a 23-ps time scale. Three-pulse photon-echo measurements showed that the correlation function of the frequency fluctuations decays on 80-fs and 1.5-ps time scales. Vibrational dephasing dynamics is close to being in a motional-narrowing limit, which can be described by a 1.6-ps pure dephasing time based on the fast-decaying component in $M(T)$. Therefore the pure dephasing process occurs on a slightly faster time scale than the depolarization dynamics. For reference, we also measured the three-pulse photon-echo signals of SCN^- in D_2O. The correlation function of the vibrational frequency fluctuation for SCN^- decays with the time constants of 80 fs and 1.3 ps. The time scales of the solvation dynamics in D_2O do not depend on the nature of vibrational mode of the solute. However the amplitudes of the correlation function depend on the system we investigated for $Fe(CN)_6^{4-}$ and SCN^-. This reflects different solute−solvent interactions which depend on the charge distribution of the solute and the form of the normal coordinates including the mode characteristics for the degenerate system.

Acknowledgment. This work was supported by a Grant-In-Aid (12304036, 13554019) from Ministry of Education, Science, Sports, and Culture, and a JSPS Research Grant for the Future Program. We thank Prof. Yasuhisa Mizutani for help with the measurement of steady-state Raman spectra and valuable discussion. K.O. is supported by the fellowship from Japan Society of Promotion for Science for Young Scientists.

References and Notes

(1) Gordon, R. G. *J. Chem. Phys.* **1965**, *43*, 1307.
(2) Rothschild, W. G. *Dynamics of Molecular Liquids*; Wiley: New York, 1984.
(3) Oxtoby, D. W. *Annu. Rev. Phys. Chem.* **1981**, *32*, 77.
(4) Oxtoby, D. W. *Adv. Chem. Phys.* **1979**, *40*, 1.
(5) Loring, R. F.; Mukamel, S. *J. Chem. Phys.* **1985**, *83*, 2116.
(6) Tokmakoff, A.; Fayer, M. D. *Acc. Chem. Res.* **1995**, *28*, 437.
(7) Fayer, M. D. *Annu. Rev. Phys. Chem.* **2001**, *52*, 315.
(8) Rector, K. D.; Fayer, M. D. In *Ultrafast Infrared, Raman Spectroscopy*; Fayer, M. D., Ed.; Marcel Dekker: New York, 2000.
(9) Fleming, G. R.; Cho, M. *Annu. Rev. Phys. Chem.* **1996**, *47*, 109.
(10) Hamm, P.; Lim M.; Hochstrasser, R. M. *Phys. Rev. Lett.* **1998**, *81*, 5326.
(11) Lim, M.; Hamm, P.; Hochstrasser, R. M. *Proc. Natl. Acad. Sci. U. S. A.* **1998**, *95*, 15315.
(12) Hamm, P.; Lim M.; Hochstrasser, R. M. *J. Phys. Chem. A* **1999**, *103*, 10049.
(13) Lim, M.; Hochstrasser, R. M. *J. Chem. Phys.* **2001**, *115*, 7629.
(14) Maekawa, H.; Ohta, K.; Tominaga, K. Submitted.
(15) Hamm, P.; Lim, M.; Hochstrasser, R. M. *J. Chem. Phys.* **1997**, *107*, 10523.
(16) Owrutsky, J. C.; Kim, Y. R.; Li, M.; Sarisky, M.; Hochstrasser, R. M. *Chem. Phys. Lett.* **1991**, *184*, 368.
(17) Li, M.; Owrutsky, J. C.; Sarisky, M.; Culver, J. P.; Yodh, A.; Hochstrasser, R. M. *J. Chem. Phys.* **1993**, *98*, 5499.
(18) Owrutsky, J. C.; Raftery, D.; Hochstrasser, R. M. *Annu. Rev. Phys. Chem.* **1994**, *45*, 519.
(19) Ferrario, M.; Klein, M. L.; MacDonald, I. R. *Chem. Phys. Lett.* **1993**, *213*, 537.
(20) Ohta, K.; Maekawa, H.; Saito, S.; Tominaga, K. *J. Phys. Chem. A* **2003**, *107*, 5643.
(21) Tokmakoff, A.; Urdahl, R. S.; Zimdars, D.; Francis, R. S.; Kwok A. S.; Fayer, M. D. *J. Chem. Phys.* **1995**, *102*, 3919.
(22) Tokmakoff, A.; Fayer, M. D. *J. Chem. Phys.* **1995**, *103*, 2810.
(23) Maekawa, H.; Tominaga, K.; Podenas, D. *Jpn. J. Appl. Phys.* **2002**, *41*, L329.
(24) Mukamel, S. *Principles of Nonlinear Optical Spectroscopy*; Oxford University: New York, 1995.
(25) Khalil, M.; Tokmakoff, A. *Chem. Phys.* **2001**, *266*, 213.
(26) Golonzka, O.; Khalil, M.; Demirdoven, N.; Tokmakoff, A. *J. Chem. Phys.* **2001**, *115*, 10814.
(27) Khalil, M.; Demirdoven, N.; Tokmakoff, A. *J. Phys. Chem.* A **2003**, *107*, 5258.
(28) Tokmakoff, A. *J. Chem. Phys.* **1996**, *105*, 1.
(29) Hamm, P.; Hochstrasser, R. M. In *Ultrafast Infrared, Raman Spectroscopy*; Fayer, M. D., Ed.; Marcel Dekker: New York, 2000.
(30) Fourkas, J. T.; Kawashima, H.; Nelson, K. A. *J. Chem. Phys.* **1995**, *103*, 4393.
(31) Jones, L. H. *Inorg. Chem.* **1963**, *2*, 777.
(32) Griffith, W. P.; Turner, G. T. *J. Chem. Soc.* **1970**, 858.
(33) Asplund, M. C.; Lim, M.; Hochstrasser, R. M. *Chem. Phys. Lett.* **2000**, *323*, 269.
(34) Merchant, K. A.; Xu, Q.-H.; Thompson, D. E.; Fayer, M. D. *J. Phys. Chem. A* **2002**, *106*, 8839.
(35) Rector, K. D.; Fayer, M. D. *J. Chem. Phys.* **1998**, *108*, 1794.
(36) Knox, R. S.; Gulen, D.; Lotterhos, K. E. *Chem. Phys. Lett.* **2002**, *361*, 285.
(37) Qian, W.; Jonas, D. M. *J. Chem. Phys.* **2003**, *119*, 1611.
(38) Tokmakoff, A.; Sauter, B.; Kwok, A. S.; Fayer, M. D. *Chem. Phys. Lett.* **1994**, *221*, 412.
(39) Park, S.-K.; Lee, C.-K.; Lee, S.-H.; Kee, N.-S. *Bull. Korean Chem. Soc.* **2002**, *23*, 253.
(40) Ohta, K.; Maekawa, H,; Tominaga, K. *Chem. Phys. Lett.*, in press.
(41) Hamm, P.; Lim, M.; Asplund, M. C.; Hochstrasser, R. M. *Chem. Phys. Lett.* **1999**, *301*, 167.
(42) Ferrario, M.; McDonald, I. R.; Symons, M. C. R. *Mol. Phys.* **1992**, *77*, 617.
(43) Rey, R.; Hynes, J. T. *J. Chem. Phys.* **1998**, *108*, 142.
(44) Ladanyi, B. M.; Stratt, R. M. *J. Chem. Phys.* **1999**, *111*, 2008.
(45) Morita, A.; Kato, S. *J. Chem. Phys.* **1998**, *109*, 5511.